Vibrational Circular Dichroism as a Probe of Fibrillogenesis: The Origin of the Anomalous Intensity Enhancement of Amyloid-like Fibrils

ARTICLE *in* JOURNAL OF THE AMERICAN CHEMICAL SOCIETY · FEBRUARY 2011

Impact Factor: 12.11 · DOI: 10.1021/ja1089827 · Source: PubMed

2 AUTHORS, INCLUDING:

Reinhard Schweitzer-Stenner
Drexel University
219 PUBLICATIONS **4,369** CITATIONS

JACS
JOURNAL OF THE AMERICAN CHEMICAL SOCIETY

ARTICLE

pubs.acs.org/JACS

Vibrational Circular Dichroism as a Probe of Fibrillogenesis: The Origin of the Anomalous Intensity Enhancement of Amyloid-like Fibrils

Thomas J. Measey and Reinhard Schweitzer-Stenner*

Department of Chemistry, Drexel University, 3201 Chestnut Street, Philadelphia, Pennsylvania 19104, United States

Supporting Information

ABSTRACT: Amyloid fibrils are affiliated with various human pathologies. Knowledge of their molecular architecture is necessary for a detailed understanding of the mechanism of fibril formation. Vibrational circular dichroism (VCD) spectroscopy has recently shown sensitivity to amyloid fibrils [Ma et al. *J. Am. Chem. Soc.* **2007**, *129*, 12364 and Measey et al. *J. Am. Chem. Soc.* **2009**, *131*, 18218]. In particular, amyloid fibrils give rise to an intensity enhanced signal in the amide I band region of the corresponding VCD spectrum, offering promise of utilizing such a method for probing fibrillogenesis and the chiral structure of fibrils. Herein, we further investigate this phenomenon and demonstrate the use of VCD to probe the fibril formation kinetics of a short alanine-rich peptide. To elucidate the origin of the anomalous VCD intensity enhancement, we use an excitonic coupling model to simulate the VCD spectrum of stacked β-sheets containing one (Ising-like model) and two amide I oscillators per strand, as models for the underlying amyloid-fibril secondary structure. With this simple model, we show that the VCD intensity enhancement of amyloid-like fibrils results from intrasheet and, to a more limited extent, also from intersheet vibrational coupling between stacked β-sheets. The enhancement requires helically twisted sheets and is most pronounced for arrangements with parallel-oriented strands. Both the intersheet distance and the orientation of the amide I transition dipole moments of neighboring sheets are found to modulate the intensity enhancement of the amide I VCD signal. Moreover, our simulations suggest that, depending on the three-dimensional arrangement of the β-strands, the sign of the VCD signal of amyloid-like fibrils can be used to distinguish between right- and left-handed helical twists of parallel-oriented β-sheets. We compare the results of our simulation to experimental spectra of two short peptides, GNNQQNY, the N-terminal peptide fragment of the yeast prion protein Sup35, and an amyloidogenic alanine-rich peptide, AKY8. Our results demonstrate the advantages of using VCD spectroscopy to probe the kinetics of peptide and protein aggregation as well as the chirality of the resulting supramolecular structure.

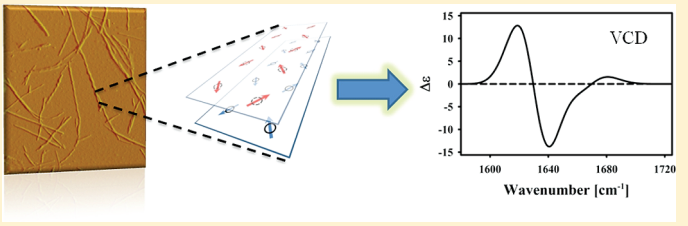

INTRODUCTION

Amyloid fibrils are the main structural constituents of intra- and extracellular proteinaceous buildup found in patients with pathologies ranging from neurodegenerative diseases such as Alzheimer's and Parkinson's diseases, to the systemic amyloidoses.[1,2] An understanding of the underlying mechanism of fibril formation is necessary for the development of diagnostic and therapeutic strategies for the various affiliated diseases.[1−3] In addition to the biomedical relevance, protein and peptide self-assembly results in the formation of supramolecular structures that can be exploited for the creation of novel biomaterials for use in various biotechnological applications.[4−6] Elucidating the mechanism of the self-assembly of peptides and proteins is therefore of utmost importance.[3]

In vitro fibril formation typical follows a nucleation mechanism, where a lag time often precedes an exponential growth of fibrillar aggregates.[1,7] Common biophysical methods employed to probe fibrillogenesis include fluorescence[8,9] and turbidity assays,[10−12] dynamic light scattering (DLS),[8,13] atomic force[14] and electron microscopic[15,16] imaging (AFM and EM, respectively), as well as vibrational spectroscopic methods such as Fourier transform infrared (FTIR)[17] and Raman[18] spectroscopies. The latter spectroscopic methods have the advantage of providing detailed structural information regarding the underlying sheet arrangement, for example, whether individual β-strands are arranged in an antiparallel or parallel fashion. Such structural information is necessary for a mechanistic understanding of fibrillogenesis on the molecular level.[19]

Recently, vibrational circular dichroism (VCD) spectroscopy has shown sensitivity to amyloid fibril structures. VCD can provide details of the chirality of the supramolecular architecture of fibrils, especially when complemented by other methods, such as IR spectroscopy.[20] Ma et al. reported the unusual intensity enhancement in the amide I region of the VCD spectra of insulin and lysozyme fibrils.[20] We recently showed that aggregation of an amyloidogenic alanine-rich octapeptide, with no known disease affiliation, produces an enhanced symmetric couplet in the corresponding VCD spectrum.[21] VCD intensity enhancement of amyloid fibrils has been suggested to originate from long-range

Received: October 15, 2010
Published: December 27, 2010

intersheet coupling with possible contributions from single sheet twisting or protofibril braiding.[20] A more recent study showed that the change in chirality of the helical twist of insulin fibrils results in a change in sign of the observed amide I′ VCD couplet.[22] It has been suggested that chirality plays a role in the onset of disease on a molecular level[22] and might have possible implications in the structural basis of different amyloid "strains".[23] Moreover, an understanding of the chirality of amyloid fibrils is of fundamental importance.[24] Clearly, reliable interpretation of the VCD signal in the amide I′ region of amyloid fibrils is necessary for its use in characterizing the chirality of the supramolecular structure of amyloid fibrils. This is the goal of the present study.

The present study contains two parts. In the first part, we briefly introduce the IR and VCD amide I spectra of two self-aggregating peptides, the recently investigated alanine-based peptide Ac−A_4KA_2Y−NH_2 (AKY8),[21] and the 7-residue N-terminal peptide fragment of the yeast prion protein Sup35, with the sequence GNNQQNY. Both show very large amide I VCD couplets, which exceed "normal" VCD signals of this mode by 2 orders of magnitude. For AKY8, we demonstrate how this "giant" VCD signal can be used to monitor the kinetics of the aggregation process. In the second part, we shed some light on the physical and structural origin and the structural determinants of the giant VCD signal by constructing a simple idealized model system, which describes a fibrillar state of a peptide in terms of stacked, helically twisted β-sheets with a rather large number of strands. Each strand contains either one or two amide I oscillators, whose orientation in the strand mimics the cases of ideal parallel and antiparallel β-sheets. Both parallel and antiparallel arrangements of strands were considered. The IR amide I band profile and the respective VCD signal were calculated for different parameters of the assumed fibril structure by utilizing a coupled oscillator approach. The merits of the excitonic coupling model to simulate the amide I band of various short peptides have been highlighted in recent years.[25−28] The model has recently been extended to simulate the amide I band profile of an aggregated alanine-rich oligopeptide.[29] By means of these calculations, we demonstrate that the VCD intensity enhancement in the amide I region results from a helical twist of long fibrils. The sign of the amide I VCD couplet depends on the handedness of the helical twist. The strength of the VCD signal depends on the distance between layers of β-sheets, the number of layers, the length of the sheets, and the strand arrangements. Hence, VCD spectroscopy emerges as a very powerful method for exploring the supramolecular structure of fibrillar peptide aggregates in the solution phase.

THEORY

Figure 1 exhibits the model system we used to simulate the amide I band profile in the IR and VCD spectra of peptide fibrils. It contains a three-dimensional lattice of amide I oscillators represented by their transition dipole moments, which were assumed to exhibit an angle of 20° with respect to the CO bond of the respective peptide group.[30] Because of the simplicity of the employed model, the term peptide group is herein used somewhat loosely, whereby it is meant to signify an amide I oscillator with a defined orientation in a string of amide I oscillators representing a polypeptide chain in a β-sheet conformation. The $m \times 2$ oscillators in the xy-plane illustrate the orientations of the transition dipole moments in an antiparallel (Figure 1a) and parallel β-sheet (Figure 1b). m is the number of strands (oriented parallel to the x-axis) built by two oscillators, and labels the

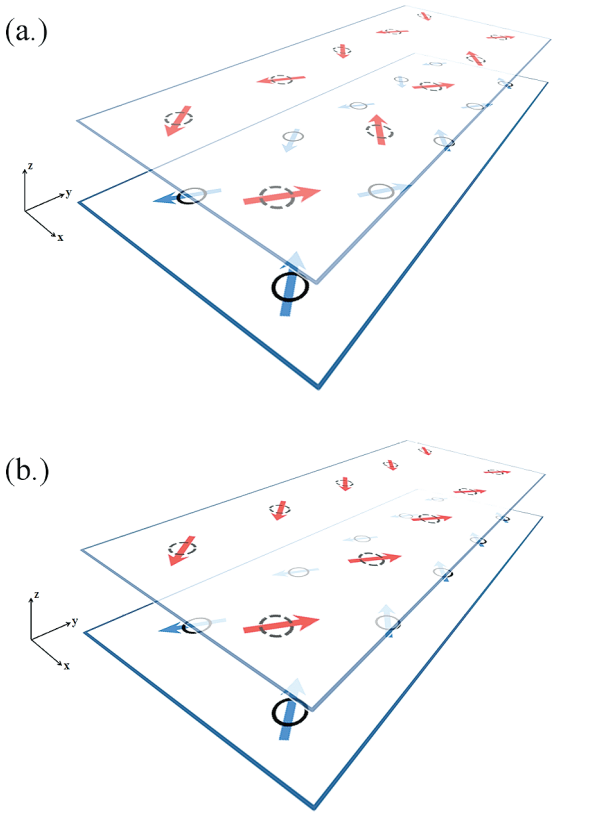

Figure 1. 3-D lattice of amide I oscillators used as a model of stacked β-sheets, where neighboring layers are oriented antiparallel to each other, and consecutive strands of the individual layers (sheets) exhibit (a) antiparallel and (b) parallel arrangements.

extension of the system in the y-direction. For technical reasons, we additionally use the term "string" for a chain of single oscillators along the y-direction. Such a string contains a single oscillator from each strand. Thus, a two-dimensional sheet contains two strings. Stacking of sheets occurs along the z-direction. In the arrangement shown in Figure 1, the two stacked sheets are oriented antiparallel to each other, but parallel orientations have also been considered in our calculations.

The Hamilton operator of N-oscillators coupled by nearest and non-nearest neighbor interactions is written as:

$$\hat{H} = \sum_{i=1}^{N} \hat{H}_i + \sum_{\substack{i,j=1 \\ i \neq j}}^{N} \hat{H}_{ij} \qquad (1)$$

where $\hat{H}_i$ is the Hamiltonian of the ith unperturbed oscillator. The interaction operator $\hat{H}_{ij}$ can generally be written as:

$$\hat{H}_{ij} = \frac{\partial^2 V}{\partial Q_i \partial Q_j} Q_i Q_j \qquad (2)$$

The product of the nuclear coordinates Q_i and Q_j of the interacting oscillators accounts for the mixing of the first excited vibrational states of the local oscillators to yield delocalized excitonic states. Herein, we count the oscillators by starting in the lower left corner of the lattice and moving along the y-axis, which coincides with the sheet direction. Hence, the last oscillator in that string is labeled as $i = m$. For subsequent counting, we move back to $y = 0$ and count the oscillators for the second string

dx.doi.org/10.1021/ja1089827 |J. Am. Chem. Soc. 2011, 133, 1066–1076

in the same *xy*-plane, which would thus run from $m + 1$ to $2m$. Next, we return to the origin ($x = y = 0$), move upward in the *z*-direction to the left string of the second layer, and continue counting in the *y*-direction, so that the first chain of oscillators in the second sheet are numbered as $2m + 1$ to $3m$. This procedure continues until we reach the upper right-hand corner, which carries the number $2mp_{max} = N$, where p_{max} is the number of one-dimensional strings in the considered lattice. *N* is thus the total number of oscillators considered

The interaction Hamiltonians for this system have been set up as follows. Interactions between oscillators in a two-oscillator strand (*x*-direction) are described by:[31]

$$\hat{H}_{i\,i+m} = \hat{H}_{i+m\,i} = 2\ \mathrm{cm}^{-1} \tag{3a}$$

Additionally, we accounted for all coupling between nearest neighbors (both interstrand and intersheet in the *y* and *z* directions, respectively) by using the transition dipole coupling formalism:[30]

$$\hat{H}_{ij} = \kappa\left(\frac{\vec{\mu}_i' \cdot \vec{\mu}_j}{|\vec{R}_{ij}|^3} - \frac{(\vec{\mu}_i' \cdot \vec{R}_{ij})(\vec{\mu}_j' \cdot \vec{R}_{ij})}{|\vec{R}_{ij}|^5}\right) \tag{3b}$$

where eq 3a accounts for nearest neighbor interaction within a two oscillator strand in the *x*-direction. κ is a constant that converts the coupling energy into cm^{-1}. $\vec{\mu}_i'$ and $\vec{\mu}_j'$ denote the two interacting dipole moments. The prime sign indicates that these are, in fact, derivatives of the ground-state electronic dipole moment with respect to the nuclear coordinate of the considered vibration (i.e., amide I). For interstrand (intrasheet) interactions, the distance $\vec{R}_{ij}$ ($j > i$) between these dipole moments reads as:

$$\vec{R}_{ij} = \begin{bmatrix} (\Delta x + \delta x)\cdot\delta_{i+m+1,j}\zeta_1 + (\Delta x - \delta x)\cdot\delta_{i+m-1,j}\xi_2 \\ \Delta y\cdot(\delta_{i+1,j}\zeta_1 + \delta_{i+m+1,j}\zeta_1 - \delta_{i+m-1,j}\zeta_2) \\ 0 \end{bmatrix} \tag{4a}$$

where

$$\zeta_1 = \begin{cases} 1; i \neq p\cdot m \\ 0; i = p\cdot m \end{cases} \text{ and } \zeta_2 = \begin{cases} 1; i \neq p'\cdot m + 1 \\ 0; i = p'\cdot m + 1 \end{cases} \tag{4b}$$

where $p = 1, 3, 5, \ldots, p_{max} - 1$ and $p' = 0, 2, 4, \ldots, p_{max} - 2$. Note that *i* runs only over the left string of a sheet. Thus, eq 4 does not account for nearest neighbor distances in the right string of a sheet. However, for our simplifying model we assumed that $R_{i+m,i+m+1} = R_{i,i+1}$. The vector components $\Delta x = 4.2$ Å and $\Delta y = 4.8$ Å are the intrastrand and interstrand distances between two oscillators, respectively. $\delta x = 1$ Å accounts for the shift between adjacent strands in an antiparallel arrangement. The respective value is zero for parallel oriented strands. $\delta_{i,j}$ is the Kronecker delta symbol. For excitonic interactions between oscillators in different sheets (layers), the distance vector can be written as:

$$\vec{R}_{ij} = \begin{bmatrix} \Delta x(\delta_{i+3m+1,j}\xi'_1 + \delta_{i+m+1,j}\xi'_2) \\ \delta y\cdot\delta_{i+2m,j} + (\Delta y + \delta y)\cdot(\delta_{i+2m+1,j} - \delta_{i,p\cdot m}) \\ -(\Delta y - \delta y)\cdot(\delta_{i+2m-1,j} - \delta_{i,p\cdot m+1} - \delta_{i,1}) \\ \Delta z(\delta_{i+2m,j} + \delta_{i+3m+1,j}\xi'_1 + \delta_{i+m+1,j}\xi'_2) \end{bmatrix} \tag{5a}$$

where

$$\xi_1 = \begin{cases} 1; p\cdot m \geq i > (p-1)\cdot m \\ 0; \mathrm{p}'\cdot m \geq i \geq (\mathrm{p}'-1)\cdot m \end{cases}$$

$$\text{and } \xi_2 = \begin{cases} 1; \mathrm{p}'\cdot m \geq i > (\mathrm{p}'-1)\cdot m > 0 \\ 0; p\cdot m \geq i > (p-1)m \end{cases} \tag{5b}$$

Note that *i* is not restricted in eq 5. The distance Δz between sheets, and the displacement parameter δy, will be used as variables for our simulations.

Diagonalizing the Hamiltonian yields the eigenvector matrix, $\hat{\alpha}$, which is needed to calculate the transition dipole moments of the excitonic states:

$$\vec{\mu}_{\mathrm{ex},i} = \sum_{i=1}^{N} \alpha_{ij}\,\vec{\mu}_j \tag{6}$$

To utilize eq 6, all dipole moments have to be rotated into the same coordinate system.[32] To this end, we use the coordinate system indicated in Figure 1. The vector representation of the dipole moment associated with the N-terminal peptide group (lower left corner) reads as:

$$\vec{\mu}_1 = \begin{pmatrix} \cos\alpha \\ \sin\alpha \\ 0 \end{pmatrix} \tag{7}$$

where $\alpha = -70°$ corresponds to an angle of 20° between the dipole moment and the CO bond. The remaining dipole moments of the system in the N-terminal coordinate system were created by the following rotational operation:

$$\vec{\mu}_{t,i}' = \vec{\mu}_1'^{T} \prod_{i=2}^{p_{max}\cdot m} A(\theta_i)\cdot B(\phi_i) \tag{8}$$

where

$$A(\theta_i) = \begin{pmatrix} \cos\theta & -(-1)^i\sin\theta & 0 \\ (-1)^i\sin\theta & \cos\theta & 0 \\ 0 & 0 & 1 \end{pmatrix} \tag{9}$$

and

$$B(\phi_i) = \begin{pmatrix} \cos\phi_i & 0 & -\sin\phi_i \\ 0 & 1 & 0 \\ \sin\phi_i & 0 & \cos\phi_i \end{pmatrix} \tag{10}$$

where ϕ_i is the angle of rotation around the *y*-axis (Figure 1) and accounts for the helical twist. $\theta = -37°$ is the angle between consecutive transition dipole moments in a string of oscillators. $\vec{\mu}_i^{\mathrm{T}}$ is the transpose of the *i*th dipole moment vector. The rotational angle for going from the end of one string ($i = p\cdot m$) to the starting point of the next one depends on whether we move between strands in a sheet ($\theta_{p\cdot m} = 143°$ if *m* is odd and 180° if *m* is even) or between strands of different layers. In the latter case, the value of $\theta_{p\cdot m}$ depends on whether we consider parallel or antiparallel arrangements of adjacent layers. In both cases, the angle between the dipole moments in a strand is 143°.

The sign of θ is negative if the respective string starts with a dipole orientation of $-70°$ (parallel to the orientation in $i = 1$), while it is positive if the orientational angle is 73°.

The VCD signal was finally calculated by using the earlier derived relation:[26]

$$R_i = \lambda \sum_{j=1}^{N} \alpha_{ij} \vec{\mu}_j' \left[\sum_{j=1}^{N} \alpha_{ij} \vec{m}_j' - \frac{i\pi}{2} \nu \sum_{j=1}^{N-2} \sum_{k=1}^{\tilde{N}-1} \vec{R}_{jk} \times (\alpha_{ij} \vec{\mu}_j' - \alpha_{ik} \vec{\mu}_k') \right] \quad (11)$$

which contributes a term containing the intrinsic magnetic dipole moment $\vec{m}_j$ of the jth residue. The wavenumber $\tilde{\nu}$ can be identified with the first moment of the IR-band profile. The constant $\lambda = 4.384 \times 10^{38}$ M cm^2 esu^2, if the dipole moments are given in units of esu cm.

For our simulation, we calculated the IR and VCD profile of amide I as an overlap of Gaussian profiles associated with the eigenenergies of the obtained excitonic states. Each function was weighted with its respective oscillator or rotational strength. The full width at half-maximum (fwhm) of each distribution was set to 10 cm^{-1}. The set of oscillators considered was assumed to be nearly degenerate, with a central intrinsic wavenumber of 1650 cm^{-1} and a small stochastic variation along the chain of ± 2 cm^{-1}. The individual electronic transition dipole moment was set to 3×10^{-19} esu cm.[33]

RESULTS AND DISCUSSION

Vibrational Spectra of Self-Aggregating Peptides. We recently reported that incubation at room temperature in the presence of HCl results in the aggregation and fibril formation of the alanine-rich octamer, Ac−(AAAAKAAY)−NH_2 (AKY8), from an unfolded ensemble of conformations.[21] Aggregation results in spectral changes of the IR amide I′ band profile that are consistent with the formation of a β-sheet structure namely,[34] a downshift of the band maximum from 1643 to 1612 cm^{-1} as shown in Figure 2a. A barely discernable band at 1695 cm^{-1} might be indicative of an antiparallel β-sheet.The amide I′ band in the polarized Raman spectra is located between the two IR active modes, ca. 1653 cm^{-1}, also consistent with an antiparallel β-sheet (Figure 2c and d).[30] The negative couplet observed in the VCD spectrum of the unaggregated peptide (not shown), which reflects a predominant fraction of polyproline II (PPII)-like conformations,[35] downshifts upon aggregation, changes sign, and is enhanced by nearly 2 orders of magnitude relative to that of the monomeric peptide as shown in Figure 2b. Here, a negative VCD couplet refers to one such that the lower energy maximum is negative and the higher energy maximum is positive. A positive couplet therefore exhibits a positive maximum at lower energy.

Intensity enhancement in the amide I region of VCD spectra of amyloid fibrils has also been recently reported by Ma et al. for lysozyme and insulin fibrils.[20] The VCD spectra obtained for these protein fibrils, however, are much less symmetric than the couplet obtained for AKY8 fibrils. As will be addressed in detail below, the sign of the VCD couplet suggests that the insulin fibrils are formed from the stacking of parallel β-sheets, in agreement with a recent study.[36] Moreover, the lack of symmetry in the couplets observed for both insulin and lysozyme fibrils might reflect intrinsic magnetic moments associated with specific amino acid residues in the protein chain, or possible irregularity in the fibril structure of larger protein systems.

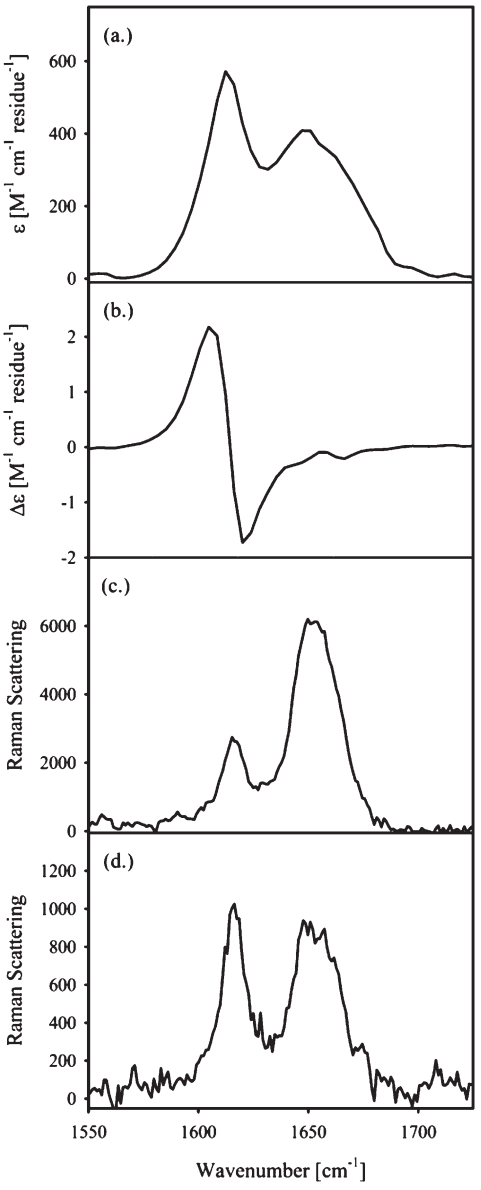

Figure 2. Amide I′ band profile in the (a) IR, (b) VCD, (c) parallel-polarized Raman, and (d) perpendicular-polarized Raman spectra of AKY8 fibril solution.

As another example, we measured the VCD and IR spectra of fibrils formed from a peptide of length similar to that of AKY8, the 7-residue N-terminal peptide fragment of the yeast prion protein Sup35, GNNQQNY. Fibrils formed from this peptide fragment are known to exhibit closely packed "dehydrated" β-sheet structures, with β-strands aligned parallel to each other and consecutive sheets arranged antiparallel.[37,38] The IR spectrum of the amide I′ band region of the GNNQQNY fibril solution has a maximum at 1630 cm^{-1}, as shown in Figure 3. The higher wavenumber position of this band, relative to that of AKY8 fibrils, suggests weaker interstrand coupling of amide I′ transition dipole moments, consistent with the notion that GNNQQNY fibrils adopt parallel β-sheets.[37,39] The polarized Raman spectra shown

dx.doi.org/10.1021/ja1089827 |J. Am. Chem. Soc. 2011, 133, 1066–1076

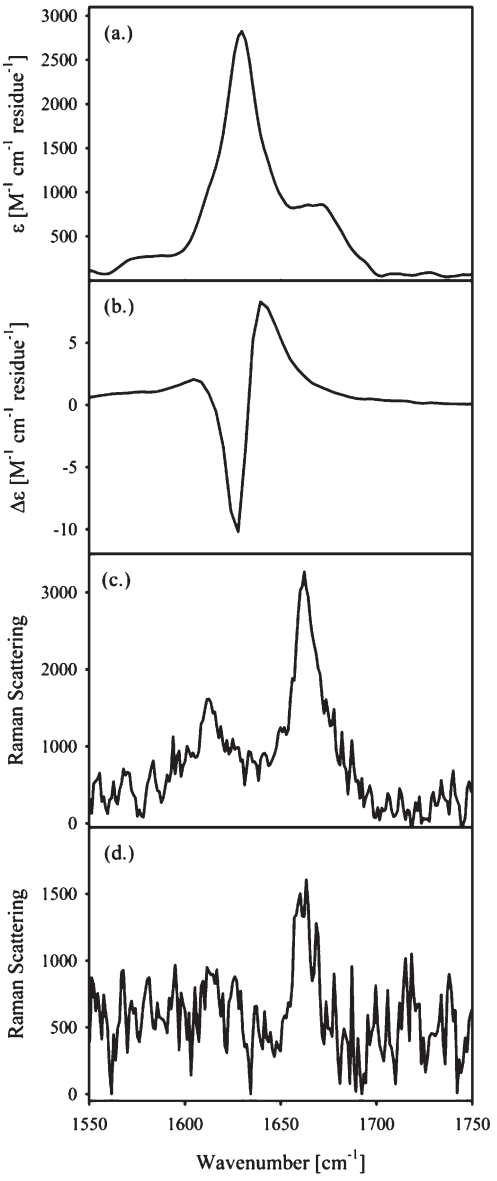

Figure 3. Amide I′ band profile in the (a) IR, (b) VCD, (c) parallel-polarized Raman, and (d) perpendicular-polarized Raman spectra of GNNQQNY fibril solution.

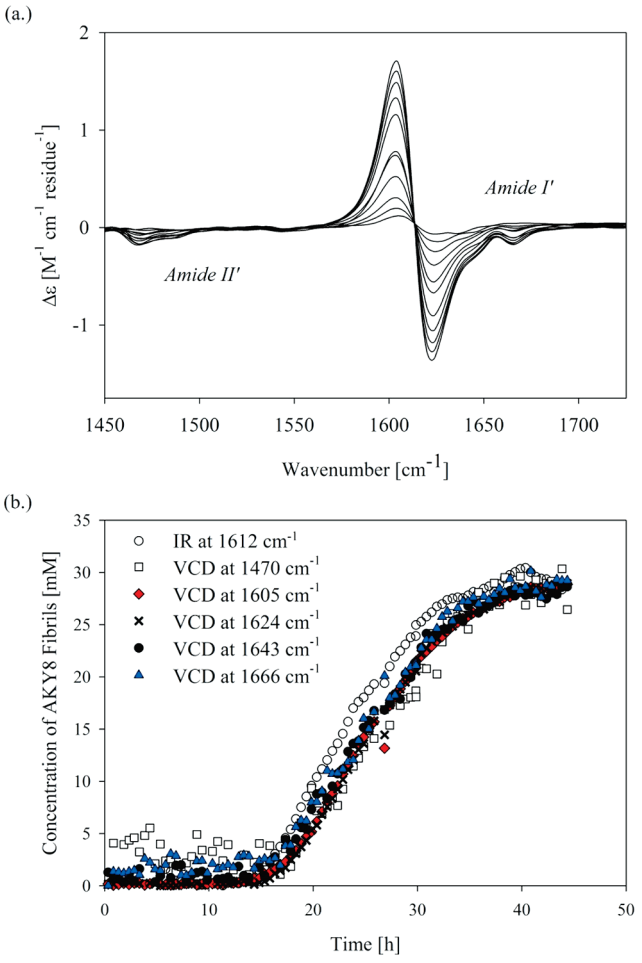

Figure 4. AKY8 fibril formation probed by VCD spectroscopy. (a) Representative time-dependent VCD spectra of a 30 mM AKY8 solution, illustrating the increase in signals in the amide I′ and amide II′ regions attributed to AKY8 fibril formation. Starting with the spectrum displaying the least intensity in the amide I′ couplet, these spectra were acquired at approximately 17, 18.5, 20, 22, 24, 26.5, 28.5, 30.5, 33.5, 37.5, and 44.5 h, respectively, after the addition of HCl. (b) Comparison of normalized fibril formation kinetics probed by IR (at 1612 cm^{-1}, ○) and various marker bands in the amide II′ and amide I′ regions of the VCD spectrum.

in Figure 3c and d show a band at approximately 1662 cm^{-1}, confirming a β-sheet secondary structure. The VCD spectrum in the amide I′ region of the GNNQQNY fibril solution exhibits an enhanced symmetric couplet, opposite in sign and nearly 5 times larger than that obtained for AKY8 fibrils (Figure 2). Moreover, the inflection point of the VCD couplet (ca. 1632 cm^{-1}) nearly coincides with the corresponding IR amide I′ maximum, confirming the higher wavenumber position of the amide I′ band, despite the contribution from Asn and Glu side chain bands, which also occur in this region.[40,41]

Because of the small absorption difference intensities associated with VCD of peptides and proteins in aqueous solution, spectra are typically acquired for a few hours to improve signal-to-noise. Because the fibrils in this case produced enhanced signals, we decided to use VCD to monitor the fibril formation kinetics of AKY8. Such time-dependent measurements would otherwise be difficult for small concentrations of peptides and proteins. In particular, we acquired multiple VCD spectra for 20 min each, immediately following addition of HCl to a solution of AKY8, which triggers the aggregation process.[21] We plotted the intensity of various marker bands in the amide II′ and amide I′ regions of the resulting VCD spectra as a function of time, as shown in Figure 4a and b. The kinetics of fibril formation (Figure 4b) show the typical sigmoidal behavior, reflective of a nucleation mechanism, where a lag period precedes an exponential growth of fibrils.[1,7] Moreover, the normalized kinetic data obtained from the intensity of different marker bands in the VCD and IR overlap nearly perfectly. This demonstrates that the enhanced VCD signals observed for amyloid-like fibrils are useful for probing fibril formation kinetics and eliminate the need for lengthy data acquisition, thereby allowing for time-resolved measurements such as the monitoring of fibril formation.

We followed the fibril formation of two different AKY8 solutions containing different peptide concentrations (20 and 30 mM) via the intensity of the positive maximum of the enhanced amide

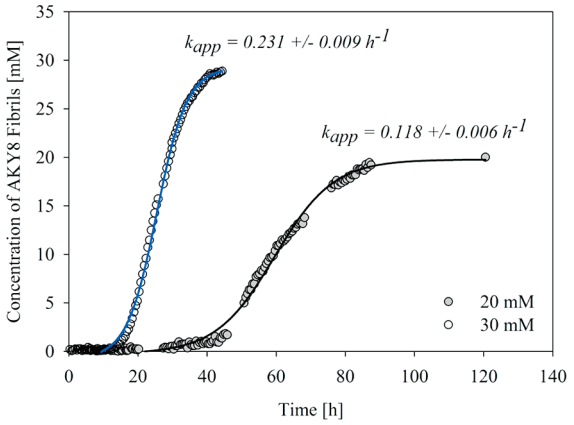

Figure 5. Comparison of the kinetics of fibril formation of 20 mM (gray ●) and 30 mM (○) AKY8 solutions, monitored via the increase in intensity of the positive maximum of the emerging VCD couplet in the amide I′ region at 1605 cm^{-1}. The data were fitted as described in the text.

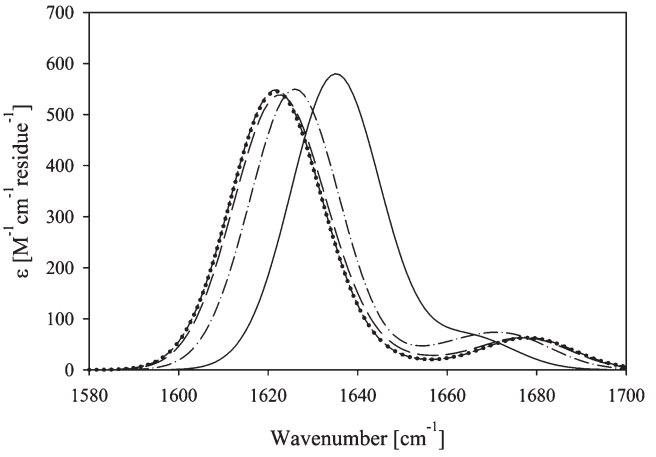

Figure 6. Simulated IR amide I band profiles based on a single-chain (Frenkel) oscillator model containing 4 (—), 8 (— — —), 12 (— · — · —), and 20 (· · ·) oscillators.

I′ couplet, as shown in Figure 5. As expected for aggregation via a nucleation mechanism, both the lag time and the apparent rate constant of fibril formation depend on the concentration of AKY8. The data were fitted with a simple sigmoidal function as described by Meng et al.[42] In particular, the lag time decreases (from 42.6 ± 0.8 to 16.8 ± 0.3 h), while the apparent first-order rate constant, k_{app}, increases (from 0.118 ± 0.006 to 0.231 ± 0.009 h^{-1}) upon increasing the peptide concentration from 20 to 30 mM. This is consistent with the in vitro aggregation of other peptides and proteins.[43−45] It should be noted that the kinetic data shown have been normalized on the concentration of the fibrils (which was assumed to have reached 100% conversion when the data plateaus), for the sake of comparing different marker bands that exhibit different extinction coefficients (see Materials and Methods).

Moreover, the apparent rate constant of the IR fibril formation kinetic data for the 30 mM AKY8 solution is 0.256 ± 0.007 h^{-1} (see Figure 4b), which is slightly higher than that obtained from the fit of the VCD kinetics using the intensity of the positive maximum of the enhanced couplet (see Figure 5). This might reflect the fact that the IR kinetics probe the formation of individual sheets, while the VCD probes the stacking of sheets to yield fibrils, as will be discussed below, and suggests that sheet formation is slightly faster than sheet stacking.

Simulation of IR and VCD Band. To elucidate the origin of the VCD intensity enhancement associated with amyloid-like fibrils, we used the oscillator chain model described in the Theory to simulate the VCD and IR band profiles of amide I for different self-aggregation scenarios. We first calculated the profiles for a single amide I oscillator string along the *y*-direction as a function of the number of oscillators. This model represents a planar β-sheet whose strands contain only a single peptide group. The result, shown in Figure 6, was obtained for dipole orientations in an antiparallel arrangement. In agreement with Lee and Cho,[33] the simulation with this simple model is already sufficient to account for the length-dependent (i.e., number of oscillators) downshift of the dominant amide I band in the IR spectrum, which is diagnostic of a β-sheet formation of self-aggregating peptides. As predicted by Lee and Cho, the length dependence levels off above 10 oscillators, so that addition of more oscillators has very little affect on the position of the amide I band. We performed the same calculations for a layer of 2*m* oscillators (2 peptides per strand), which yielded practically the same result. Because all of the oscillators are in a single plane, there is no VCD signal for these scenarios (data not shown). However, because real β-sheets are not totally flat, a very weak VCD signal at the position of the strongest amide I band is normally observed.[46,47]

In a second step, we calculated the IR and VCD profiles for the following model of peptide fibrils. We assumed the stacking of three layers of 20 strands containing 2 × 20 oscillators. The distance between the layers, which were assumed to be in register, was set to 10 Å. The term "in register" means that corresponding oscillators of different layers differ only in their *z*-coordinate. In a first step, we considered the following arrangements: (a) *aa*, where adjacent strands are all antiparallel to each other and neighboring sheets represented by adjacent layers of oscillators are also arranged antiparallel to each other (Figure 1a), (b) *ap*, for which the arrangement in a layer is antiparallel, whereas sheets are oriented parallel to each other (Figure 1b), (c) *pa*, which exhibits parallel β-sheets with antiparallel oriented layers, and (d) *pp*, in which arrangements between both strands and sheets are parallel. This set represents four of the eight possible arrangements listed by Sawaya et al.[48] They have in common that they all exhibit a face-to-back orientation of adjacent layers. For each of these arrangements, we considered a network of 2(x) × 20(y) × 3(z) oscillators (i.e., 3 sheets with 20 strands per sheet and 2 oscillators per strand). The corresponding IR spectra resemble very well what one would expect for antiparallel (in *aa* and *ap*) and parallel (in *pa* and *pp*) sheets (Figure S1 in the Supporting Information). The former shows a weak band at higher wavenumbers, which is hardly discernible in the spectrum of the latter. As expected, there is still no VCD signal because the fibrils do not exhibit any chirality. These results suggest that in register stacking has a very small influence on the amide I band profile of β-sheets.

In the next step, we assumed a twist of ±2° per strand, which produces left-handed (+) and right-handed (−) helical structures. The helical axis coincides with the *y*-axis. Figure 7 exhibits the amide I profiles for the above introduced arrangements. The VCD signals obtained for *aa* and *ap* are comparatively weak. While they exhibit the couplet-like features also depicted in the experimental spectra displayed in Figures 2 and 3, their intensities do not exceed those of VCD signals obtained for normal

dx.doi.org/10.1021/ja1089827 |J. Am. Chem. Soc. 2011, 133, 1066–1076

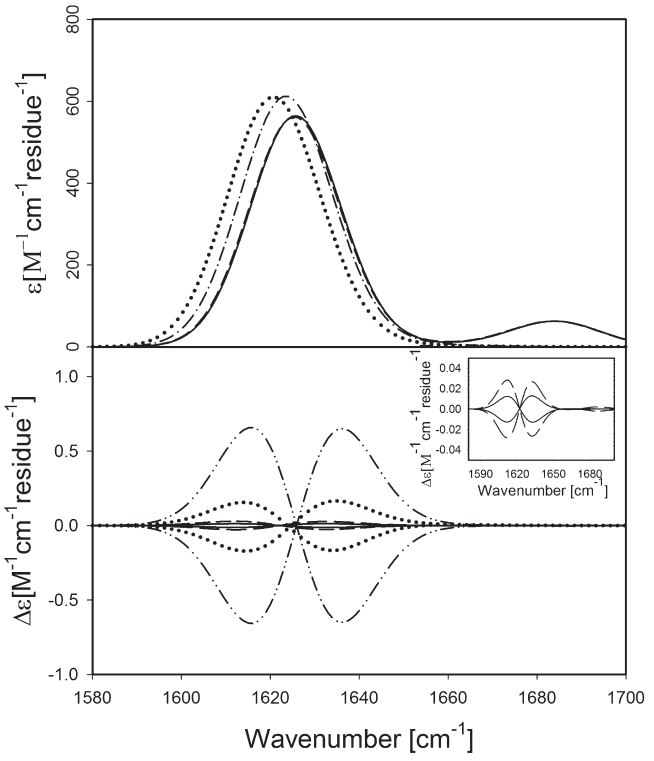

Figure 7. Simulated IR (top) and VCD (bottom) amide I band profiles for the *aa* (—), *ap* (– – –), *pp* (— · — · —), and *pa* (· · ·) configurations of strings and layers. Three layers of 2 × 20 oscillators were considered. The distance between sheets was 10 Å. Helical twists of ±2° yielded the negative and positive couplets, which are described in detail in the text. The inset shows an enlarged representation of the VCD couplets calculated for *aa* (—) and *ap* (– – –).

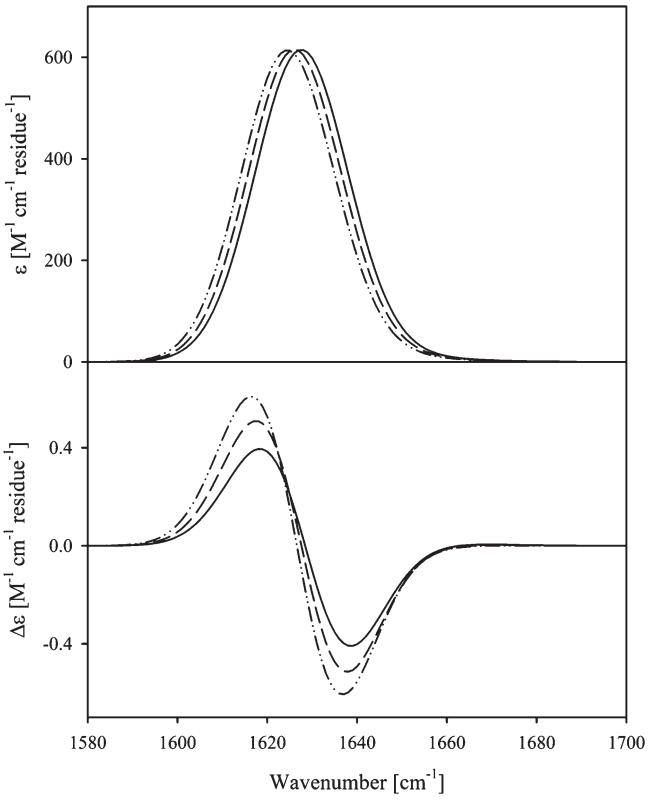

Figure 8. Simulated IR (top) and VCD (bottom) amide I band profiles for the *pp* arrangements of strings and layers calculated for three different interlayer distances, 8 Å (—), 10 Å (– – –), and 15 Å (— · — · —). Three layers of 2 × 20 oscillators were considered. A helical twist of +2° was assumed.

secondary structures like α-helices, *β*-strands, polyproline II helices, and turns.[46,49] The VCD signal obtained for the *pa* arrangement is a factor of 2 stronger than that of *aa*. The VCD spectra in the amide I region of *pa* and *pp*, however, clearly display an enhanced couplet centered at the position of the (low wavenumber) amide I band, which is an order of magnitude larger than what one generally obtains for all types of secondary structures.[50] For a left-handed helical twist, which is predominant among peptide fibrils,[51] the couplets are all positive. As expected, a right-handed twist causes a reversal in the sign of the couplet.

We explored how the intensities of the couplets change as a function of the number of layers and the (intersheet) distance between them. For the *pa* arrangement, the results are shown in Figures S2—S4 in the Supporting Information. The couplet intensities of all four arrangements were found to increase with increasing sheet (layer) length, indicating that long twisted fibrils can give rise to rather large couplets (cf. Figure S4 for *pa*). The VCD-signals of *ap* and *pa* do not depend on the distance between layers, indicating that the respective VCD couplets solely reflect the intrinsic chirality of the individual sheets. Interestingly, the VCD signals of *aa* and *pp* decrease with decreasing interlayer distance, which suggests that intersheet excitonic coupling reduces the rotational strength of amide I. This is illustrated in Figure 8, which shows the IR and VCD amide I profiles of the *pp*-arrangement of a 2 × 20 × 3 lattice for the three interlayer distances of 8, 10, and 15 Å. The influence of the number of layers (sheets) on the VCD signal is quite different for the four arrangements. For *aa*, the couplet was found to decrease with an increasing number of sheets, while it clearly increases for *pp*. It (modestly) increases for *ap*. The *pa* arrangement shows a rather peculiar behavior in that the sign of the couplet depends on the number of layers. In particular, the sign of the couplet is positive for an odd numbers of sheets (as shown in Figure 7), but negative for even numbers. Additionally, the magnitude of the couplet increases with an increasing number of layers. Figure S2 exhibits the IR and VCD profiles for a 2 × 20 × *q* lattice with *q* = 2—4.

To quantitatively account for our experimentally measured VCD signals, we first consider GNNQQNY and its fibril structure reported by Nelson et al.[38] We calculated the VCD and IR amide I band of a double layer of 2 × 200 oscillators, which would correspond to a fibril of ca. 96 nm in length. This is still a comparatively short fibril. The interlayer distance was set to 8.5 Å, in accordance with what Nelson et al.[38] reported for sheets with dry interfaces in the core of GNNQQNY fibrils, which were found to exhibit alternating dry and wet (filled with H_2O) interfaces. The latter have an interlayer distance of 15 Å. To account for the observed negative couplet, we used a helical twist of 2°. The result of our calculation is shown in Figure 9 (solid line). The VCD signal is significantly enhanced, but still weaker than the experimental one displayed in Figure 3. An even stronger signal could easily be achieved by considering longer fibrils. Alternatively, one might assume a somewhat heterogeneous structure, which leads to a statistical variation of the transition dipole moment's orientation angle by ±3°. This yields a strong VCD couplet even for the rather short sheet length considered in this calculation, which is close to the experimental value observed for

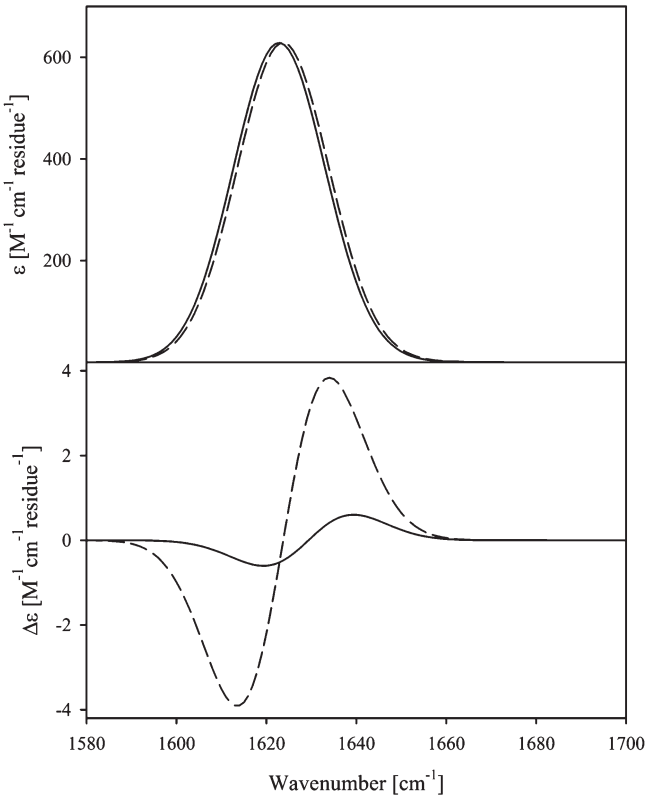

Figure 9. Simulated IR (top) and VCD (bottom) amide I bands profiles for a double layer of 2 × 200 oscillators with a *pa* configuration resembling the structural properties of GNNQQNY fibrils as described in the text. The distance between the layers was assumed to be 8.5 Å. The two sheets were assumed to be displaced by 2.4 Å along the fibril axes (y) to account for the experimentally observed zipper-like stacking.[38] The solid line band profiles were calculated for a helical twist of 2°; for the dashed-line profile, we additionally assumed a heterogeneity of the transition dipole orientation of ±3°.

the Sup35 fragment (dashed line in Figure 9). These results show that a fibril geometry similar to that reported by Nelson et al.[38] can indeed produce a very large negative VCD couplet of the amide I mode if we allow some left-handed helical twisting in the fibril structure.

The results presented thus far seem to suggest that a "giant" VCD is indicative of fibrils with parallel β-sheets. The strongly enhanced positive couplet observed for a left-handed twist of the *pp* arrangement may seem like a perfect model for the underlying β-sheet architecture of AKY8 fibrils (Figures 7 and 8). A difficulty with this model, however, arises from the fact that a *pp* arrangement of AKY8 would bring the two charged lysines into close proximity for an in-register β-sheet, which would have a destabilizing effect. However, one could think about an arrangement in which different layers are not in register, so that the tyrosine in one layer is positioned right between the lysines of two adjacent layers, such as:

AAAAKAAY
AAAAKAAY
AAAAKAAY

where the nonitalic characters represents a strand in a shifted sheet (along x and y) stacked onto the sheet represented by the characters in italics.

The low wavenumber position of the most intense amide I band in the experimental IR spectrum of AKY8 seems to indicate an antiparallel β-sheet arrangement. However, our calculations show that in twisted fibrils, a parallel arrangement does not necessarily lead to a less pronounced downshift of the dominant amide I peak. The results of our calculations, shown in Figure 7, rather suggest that the occurrence of the weak high-wavenumber band is the decisive fingerprint for an antiparallel structure. The existence of such a band cannot unambiguously be discerned from the spectrum in Figure 2, due to the broad band in the 1640−1650 cm^{-1} region, which reflects fibrils with a disordered local structure.[21] If the sheets of AKY8 are indeed built by antiparallel strands, π stacking between tyrosines or π-cation interactions between the tyrosine and lysine side chains of strands in adjacent sheets require a 180° rotation around an axis parallel to the x-axis, which connects the center of the two dipole moments of a strand, as shown in Figure S5 for two AKY8 strands. For this scenario, an in-register arrangement of the two strands termed aa^r (where the superscript r denotes the strand with the 180° rotation) would allow for π stacking between the tyrosines, whereas π-cation interactions between the lysine and tyrosine residues require the following out-of-register arrangement:

AAAAKAAY
YAAKAAAA

This mode of interaction has been proposed in our earlier paper.[21] The respective arrangement corresponds to what Sawaya et al. termed as antiparallel face-to-face arrangement, which they introduced as hypothetical and "not yet observed".[48]

To investigate whether peptide aggregation into fibrils with an aa^r arrangement can indeed cause a positive couplet of the magnitude observed for AKY8, we calculated the amide I profiles for two double layer lattices of different lengths, containing 2 × 80 and 2 × 120 oscillators per layer. To account for the observed left-handed twist of AKY8 fibrils, we assume a helical twist of 2° per strand. As shown in Figure 10, this yields a modestly enhanced positive couplet, which is a factor of 10 larger than conventional amide I VCD signals. However, as one can already infer from a comparison of the two simulations, the longer lattice results in a slightly weaker signal. Additional calculations show that the signal decreases further with increasing chain length and changes sign if the length exceeds 250 oscillators. Such a periodic variation of the VCD signal was also obtained for *pa*, but not for the remaining arrangements. Our calculations do not rule out that aa^r is a good candidate for AKY8 (in fact, it is the only one if the sheet arrangement is indeed antiparallel), but this would mean that the AKY8 fibrils are of the necessary length required to produce a positive VCD couplet.

It is interesting to also note the enhanced asymmetric positive couplet recently observed for insulin fibrils by Ma et al.[20] On the basis of the results of our simulation, we would expect the underlying fibril architecture to result from the stacking of parallel β-sheets. Indeed, Zako et al. suggested that insulin fibrils are comprised of parallel sheets, based on ATR-IR spectra, thus further reinforcing the results of our VCD simulations.[36]

Excitonic coupling in a system of so many nearly degenerate oscillators gives rise to a broad spectrum with a high and nearly constant density of excitonic states, as shown in more detail in the Supporting Information. In particular, the strong bands in the IR spectrum and the VCD couplet of such a degenerate oscillator

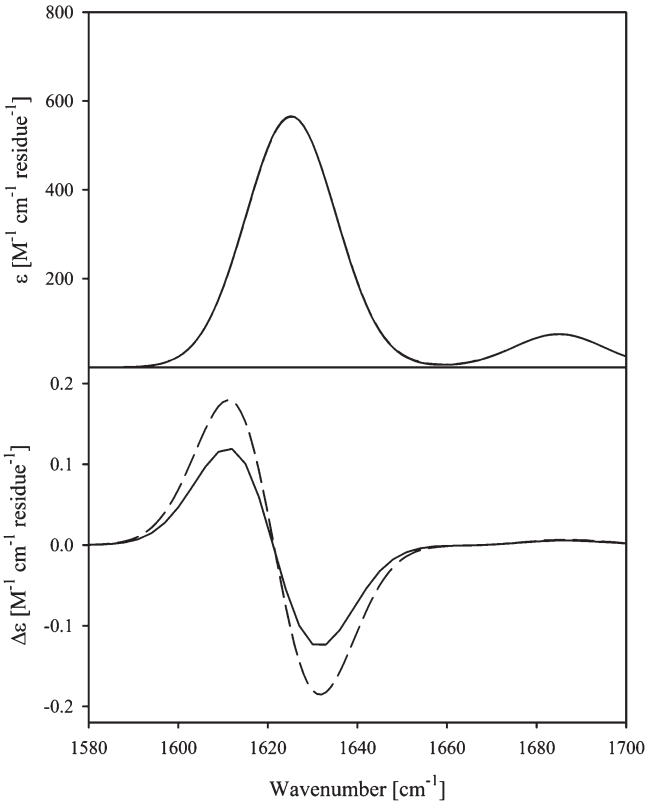

Figure 10. Simulated IR (top) and VCD (bottom) amide I bands profiles for a lattice containing 2 layers of 2 × 120 oscillators (—) and 2 × 80 oscillators (— — —) in an *aa*′ arrangement. The distance between layers was 10 Å. A left-handed helical twist of 2° per strand was considered.

model are built mostly by contributions from only two excitonic transitions (Figure S7). A change of the still rather regular geometry of the model would lead to a broader distribution of intensities, particularly in the region between the two bands obtained for the *aa* configuration.[29] This could explain the asymmetric couplets observed for fibrils of larger systems, such as insulin and lysozyme, obtained by Ma et al.[20]

CONCLUSION

We have demonstrated the use of VCD to probe the fibril formation kinetics of a short amyloidogenic peptide. Fibril formation results in an enhanced signal in the amide I region of the corresponding VCD spectrum. Such an intensity enhancement can allow for measurements of samples that aggregate at particularly low concentrations. These results add VCD spectroscopy to the arsenal of biophysical methods available to probe fibrillogenesis.

Using a simplified model of the stacked β-sheet structure of amyloid fibrils, we showed that the VCD intensity enhancement observed for such fibrils results from intrasheet and, to a more limited extent, also from intersheet interactions. The sign of the couplet depends on the handedness of the twist, the relative orientation of the strands in a three-dimensional fibril, and, in the case of the *pa* arrangement, also on the number of stacked sheets in a fibril. For fibrils comprised of antiparallel β-sheets, a modified *aa* arrangement, in which every other strand in one sheet of a double-layer subunit is rotated by 180° about their strand (x) axes, can produce an enhanced positive couplet at the position of the low-wavenumber band in the IR spectrum. For fibrils exhibiting *pp* and *pa* arrangements, helical twisting is necessary and sufficient to produce such a strong VCD couplet at the low-wavenumber band position. The VCD spectrum of the Sup35 fragment suggests a (small) left-handed twist. Few methods are currently available that exhibit the ability to provide such structural detail about amyloid fibrils.[19] It is interesting to note that insulin fibrils exhibit a VCD signal similar in sign to that obtained for GNNQQNY fibrils, although the former is somewhat asymmetric. In fact, both insulin[36] and GNNQQNY fibrils are known to be comprised of parallel β-sheets.[38]

Despite the simplicity of the employed model, which does not provide a detailed structural representation of a real β-sheet, it should be considered as reliable in that it catches the essential properties of stacked β-sheets, which give rise to the observed spectral features, that is, a clear downshift of the first moment of amide I and a "giant" VCD signal. Our results are in line with findings of Lee and Cho, who demonstrated that a linear chain of hydrogen-bonded residues in consecutive "pseudo-β-sheets" is sufficient to construct the Frenkel exciton Hamiltonian used to simulate the amide I band profile in the IR spectra of β-sheets containing different numbers of strands, reproducing the red-shift of the amide I as a function of the number of strands.[33]

Taken together, this study provides the theoretical framework for simulating the VCD spectra of amyloid fibrils and confirms that the origin of the anomalous intensity enhancement results predominantly from intrasheet and, to a lesser extent, from intersheet excitonic coupling. VCD spectroscopy is now emerging as a novel biophysical method to probe the structure and kinetics of amyloid fibrils, and future VCD studies will be sure to add insight to the biomedically and biotechnologically important phenomenon of amyloid fibril formation.

MATERIALS AND METHODS

Materials. Ac—(AAAAKAAY)—NH_2 (AKY8) was custom synthesized by Celtek Peptides (Nashville, TN). The peptide was dialyzed in a Spectra-Por Float-A-Lyzer Dialysis Bag with a molecular weight cutoff of 500 Da (Spectrum Laboratories), to remove residual trifluoroacetic acid (TFA), which overlaps with the amide I′ band in the FTIR spectrum. The peptides were then lyophilized overnight and redissolved in D_2O. For AKY8, the exact peptide concentration was determined from the tyrosine $\pi \rightarrow \pi^*$ absorption at 275 nm, which has an extinction coefficient of 1450 M^{-1} cm^{-1}, for experiments involving the monomeric, nonaggregated state.[52] To form the fibril solution of AKY8, the peptide was incubated overnight at room temperature in the presence of deuterium chloride (DCl). This procedure resulted in a gelatinous solution, containing AKY8 fibrils.

The 7-residue peptide motif from the N-terminal region of the yeast prion protein Sup35, GNNQQNY, was purchased from AnaSpec (Fremont, CA) and was used without further purification. The peptide was dissolved in D_2O at a concentration between 1 and 2 mg/mL and allowed to incubate at room temperature overnight. These conditions promote the aggregation of GNNQQNY into amyloid-like fibrils and microcrystals.[53,54]

VCD and FTIR Spectroscopy. Vibrational circular dichroism (VCD) and FTIR spectra were measured with a ChiralIR spectrometer with a single PEM from BioTools (Jupiter, FL). The peptide solutions were placed in either a 20 μm or a 56 μm CaF_2 BioCell obtained from BioTools. The VCD and IR spectra were collected using the ChiralIR software implemented in GRAMS/AI software v. 7.00 (Thermo Galactic). The VCD and IR spectra of the supernatant fibril solutions

of both AKY8 and GNNQQNY were obtained for 18 and 2 min, respectively. Both VCD and IR spectra were collected using 8 cm^{-1} resolution.

Kinetic VCD and IR experiments were carried out using the features of the ChiralIR software, which allowed for arrayed or "blocked" experiments. For all VCD and IR kinetic experiments, 20 min blocks were measured, where, for each block, the VCD and IR spectra were acquired for 18 and 2 min, respectively. To compare the kinetics probed for different AKY8 concentrations and at different VCD and IR marker bands, all spectra were normalized on the concentration of fibrils. For the sake of comparison, the aggregation was assumed reach to 100% completion, so that the maximum intensity was set to either 20 or 30 mM, depending on the initial AKY8 stock solution that was used. Because only a relative comparison was made in this Article, we feel that such an approach is justified. Following Meng et al., the kinetic data were fitted with a simple sigmoidal function.[42]

Polarized Raman Spectroscopy. The polarized Raman spectra of AKY8 and GNNQQNY were obtained with the 514 nm excitation from a mixed-gas ArKr laser (Stabilite 2018-RM). The laser beam was directed into a RM 100 Renishaw confocal Raman microscope and focused onto a 1.0 mm Q Silica microscope slide, upon which a drop of the peptide fibril solution was placed. The scattered light was filtered with a 514 nm notch filter, dispersed by a single-grating 2400 L/mm grating, and imaged onto a back-thinned Wright Instrument CCD. It was polarized by a combination of a linear polarizer and a $\lambda/2$ plate. The latter rotates the *y*-polarized light (perpendicular to the laser polarization) into the *x*-direction to achieve an optimal spectrometer transmission. All spectra were recorded in the "continuous" mode. Two scans were measured for the AKY8 and GNNQQNY fibril solutions for both polarizations, and the spectra were averaged for each polarization direction to eliminate some of the noise.

■ ASSOCIATED CONTENT

Supporting Information. Calculated VCD and IR spectra as a function of various parameters. This material is available free of charge via the Internet at http://pubs.acs.org.

■ AUTHOR INFORMATION

Corresponding Author
rschweitzer-stenner@drexel.edu

■ ACKNOWLEDGMENT

We would like to thank Larry Nafie for helpful discussions and for providing us with a preprint of his manuscript (Kurouski et al. *Chem. Commun.* **2010**, *46*, 7154). This work was supported by the NSF (Chem 0804492) to R.S.-S.

■ REFERENCES

(1) Chiti, F.; Dobson, C. M. *Annu. Rev. Biochem.* **2006,** *75*, 333.
(2) Dobson, C. M. *Trends Biochem. Sci.* **1999,** *24*, 329.
(3) Dobson, C. M. *Nature* **2003,** *426*, 884.
(4) Yokoi, H.; Kinoshita, T.; Zhang, S. *Proc. Natl. Acad. Sci. U.S.A.* **2005,** *102*, 8414.
(5) Hamley, I. W. *Angew. Chem., Int. Ed.* **2007,** *46*, 8128.
(6) Zhang, S.; Altman, M. *React. Funct. Polym.* **1999,** *41*, 91.
(7) Gazit, E. *Angew. Chem., Int. Ed.* **2002,** *41*, 257.
(8) Modler, A. J.; Gast, K.; Lutsch, G.; Damaschun, G. *J. Mol. Biol.* **2003,** *325*, 135.
(9) LeVine, H., III. *Protein Sci.* **1993,** *2*, 404.
(10) Wood, S. J.; Maleeff, B.; Hart, T.; Wetzel, R. *J. Mol. Biol.* **1996,** *256*, 870.
(11) Jarrett, J. T.; Lansbury, P. T., Jr. *Biochemistry* **1992,** *31*, 12345.
(12) Wood, S. J.; Chan, W.; Wetzel, R. *Chem. Biol.* **1996,** *3*, 949.
(13) Walsh, D. M.; Lomakin, A.; Benedek, G. B.; Condron, M. M.; Teplow, D. B. *J. Biol. Chem.* **1997,** *272*, 22364.
(14) Harper, J. D.; Wong, S. S.; Lieber, C. M.; Lansbury, P. T., Jr. *Chem. Biol.* **1997,** *4*, 119.
(15) Makin, O. S.; Serpell, L. C. *J. Mol. Biol.* **2004,** *335*, 1279.
(16) Goldsbury, C. S.; Cooper, G. J. S.; Goldie, K. N.; Müller, S. A.; Saafi, E. L.; Gruijters, W. T. M.; Misur, M. P.; Engel, A.; Aebi, U.; Kistler, J. *J. Struct. Biol.* **1997,** *119*, 17.
(17) Zandomeneghi, G.; Krebs, M. R. H.; McCammon, M. G.; Fändrich, M. *Protein Sci.* **2004,** *13*, 3314.
(18) Shashilov, V. A.; Lednev, I. K. *J. Am. Chem. Soc.* **2008,** *130*, 309.
(19) Popova, L. A.; Kodali, R.; Wetzel, R.; Lednev, I. K. *J. Am. Chem. Soc.* **2010,** *132*, 6324.
(20) Ma, S.; Cao, X.; Mak, M.; Sadik, A.; Walkner, C.; Freedman, T. B.; Lednev, I. K.; Dukor, R. K.; Nafie, L. A. *J. Am. Chem. Soc.* **2007,** *129*, 12364.
(21) Measey, T. J.; Smith, K. B.; Decatur, S. M.; Zhao, L.; Yang, G.; Schweitzer-Stenner, R. *J. Am. Chem. Soc.* **2009,** *131*, 18218.
(22) Kurouski, D.; Lombardi, R. A.; Dukor, R. K.; Lednev, I. K.; Nafie, L. A. *Chem. Commun.* **2010,** *46*, 7154.
(23) Dzwolak, W.; Loksztejn, A.; Galinska-Rakoczy, A.; Adachi, R.; Goto, Y.; Rupnicki, L. *J. Am. Chem. Soc.* **2007,** *129*, 7517.
(24) Rubin, N.; Perugia, E.; Goldschmidt, M.; Fridkin, M.; Addadi, L. *J. Am. Chem. Soc.* **2008,** *130*, 4602.
(25) Hagarman, A.; Measey, T. J.; Mathieu, D.; Schwalbe, H.; Schweitzer-Stenner, R. *J. Am. Chem. Soc.* **2010,** *132*, 540.
(26) Schweitzer-Stenner, R. *J. Phys. Chem. B* **2004,** *108*, 16965.
(27) Eker, F.; Griebenow, K.; Cao, X.; Nafie, L. A.; Schweitzer-Stenner, R. *Proc. Natl. Acad. Sci. U.S.A.* **2004,** *101*, 10054.
(28) Schweitzer-Stenner, R.; Measey, T. J. *Proc. Natl. Acad. Sci. U.S.A.* **2007,** *104*, 6649.
(29) Schweitzer-Stenner, R.; Measey, T. J. *Spectroscopy* **2010,** *24*, 25.
(30) Krimm, S.; Bandekar, K. *Adv. Protein Chem.* **1986,** *38*, 181.
(31) Schweitzer-Stenner, R. *J. Phys. Chem. B* **2009,** *113*, 2922.
(32) Schweitzer-Stenner, R. *Vib. Spectrosc.* **2006,** *42*, 98.
(33) Lee, C.; Cho, M. *J. Phys. Chem. B* **2004,** *108*, 20397.
(34) Barth, A. *Biochim. Biophys. Acta* **2007,** *1767*, 1073.
(35) Measey, T.; Schweitzer-Stenner, R. *Chem. Phys. Lett.* **2005,** *408*, 123.
(36) Zako, T.; Sakono, M.; Hasimoto, N.; Ihara, M.; Maeda, M. *Biophys. J.* **2009,** *96*, 3331.
(37) Balbirnie, M.; Grothe, R.; Eisenberg, D. S. *Proc. Natl. Acad. Sci. U.S.A.* **2001,** *98*, 2375.
(38) Nelson, R.; Sawaya, M. R.; Balbirnie, M.; Madsen, A. Ø.; Riekel, C.; Grothe, R.; Eisenberg, D. *Nature* **2005,** *435*, 773.
(39) Reddy, A. S.; Chopra, M.; de Pablo, J. J. *Biophys. J.* **2010,** *98*, 1038.
(40) Measey, T.; Hagarman, A.; Eker, F.; Griebenow, K.; Schweitzer-Stenner, R. *J. Phys. Chem. B* **2005,** *109*, 8195.
(41) Venyaminov, S. Y.; Kalnin, N. N. *Biopolymers* **1990,** *30*, 1243.
(42) Meng, X.; Munishkina, L. A.; Fink, A. L.; Uversky, V. N. *Biochemistry* **2009,** *48*, 8206.
(43) Caughey, B.; Lansbury, P. T., Jr. *Annu. Rev. Neurosci.* **2003,** *26*, 267.
(44) Bitan, G.; Kirkitadze, M. D.; Lomakin, A.; Vollers, S. S.; Benedek, G. B.; Teplow, D. B. *Proc. Natl. Acad. Sci. U.S.A.* **2002,** *100*, 330.
(45) Perutz, M. F.; Windle, A. H. *Nature* **2001,** *412*, 143.
(46) Keiderling, T. A. *Nature* **1986,** *322*, 851.
(47) Measey, T. J.; Schweitzer-Stenner, R. *J. Am. Chem. Soc.* **2006,** *128*, 13324.
(48) Sawaya, M. R.; Samashivan, S.; Nelson, R.; Ivanova, M. I.; Sievers, S. A.; Apostol, M. I.; Thompson, M. J.; Balbirnie, M.; Wiltzius, J. J. W.; Farlane, H. T.; Madsen, A. Ø.; Riekel, C.; Eisenberg, D. *Nature* **2007,** *447*, 453.
(49) Bour, P.; Keiderling, T. A. *J. Am. Chem. Soc.* **1993,** *115*, 9602.

(50) Keiderling, T. A. *Curr. Opin. Chem. Biol.* **2002,** *6*, 682.
(51) Jiménez, J. L.; Nettleton, E. J.; Bouchard, M.; Robinson, C. V.; Dobson, C. M.; Saibil, H. R. *Proc. Natl. Acad. Sci. U.S.A.* **2002,** *99*, 9196.
(52) Decatur, S. M.; Antonic, J. *J. Am. Chem. Soc.* **1999,** *121*, 11914.
(53) Marshall, K. E.; Hicks, M. R.; Williams, T. L.; Hoffman, S. V.; Rodger, A.; Dafforn, T. R.; Serpell, L. C. *Biophys. J.* **2010,** *98*, 330.
(54) van der Wel, P. C. A.; Lewandowski, J. R.; Griffin, R. G. *J. Am. Chem. Soc.* **2007,** *129*, 5117.